

# REVIEWS

## Modeling the membrane environment has implications for membrane protein structure and function: Influenza A M2 protein

Huan-Xiang Zhou,<sup>1,2</sup> and Timothy A. Cross<sup>2,3,4\*</sup>

<sup>1</sup>Department of Physics, Florida State University, Tallahassee, Florida 32306

<sup>2</sup>Institute of Molecular Biophysics, Florida State University, Tallahassee, Florida 32306

<sup>3</sup>Department of Chemistry and Biochemistry, Florida State University, Tallahassee, Florida 32306

<sup>4</sup>National High Magnetic Field Laboratory, Florida State University, Tallahassee, Florida 32306

Received 26 November 2012; Revised 29 January 2013; Accepted 30 January 2013

DOI: 10.1002/pro.2232

Published online 7 February 2013 proteinscience.org

**Abstract:** The M2 protein, a proton channel, from Influenza A has been structurally characterized by X-ray diffraction and by solution and solid-state NMR spectroscopy in a variety of membrane mimetic environments. These structures show substantial backbone differences even though they all present a left-handed tetrameric helical bundle for the transmembrane domain. Variations in the helix tilt influence drug binding and the chemistry of the histidine tetrad responsible for acid activation, proton selectivity and transport. Some of the major structural differences do not arise from the lack of precision, but instead can be traced to the influences of the membrane mimetic environments. The structure in lipid bilayers displays unique chemistry for the histidine tetrad, which binds two protons cooperatively to form a pair of imidazole-imidazolium dimers. The resulting interhistidine hydrogen bonds contribute to a three orders of magnitude enhancement in tetramer stability. Integration with computation has provided detailed understanding of the functional mechanism for proton selectivity, conductance and gating of this important drug target.

**Keywords:** membrane proteins; membrane mimetics; M2 proton channel; Influenza A; molecular dynamics simulations; QM/MM calculations; solid state NMR; conductance mechanism

---

\*Correspondence to: Timothy A. Cross, National High Magnetic Field Lab, 1800 E. Paul Dirac Dr., Tallahassee, FL 32310. E-mail: cross@magnet.fsu.edu.

Grant sponsor: National Institutes of Health through Grants; Grant number: AI-074805, GM-088187; Grant sponsor: National Science Foundation through Cooperative Agreement between the Division of Materials Research and the State of Florida; Grant number: 0654118.

### Introduction

Helical membrane proteins have presented a great challenge for structural biology because of their weak tertiary/quaternary structural stability, as well as the difficulties associated with protein expression, purification and sample preparation. The weak tertiary/quaternary structural stability is a result of their highly hydrophobic amino acid compositions in the transmembrane (TM) domains and the uniformity of the secondary structure.<sup>1,2</sup> With the amide

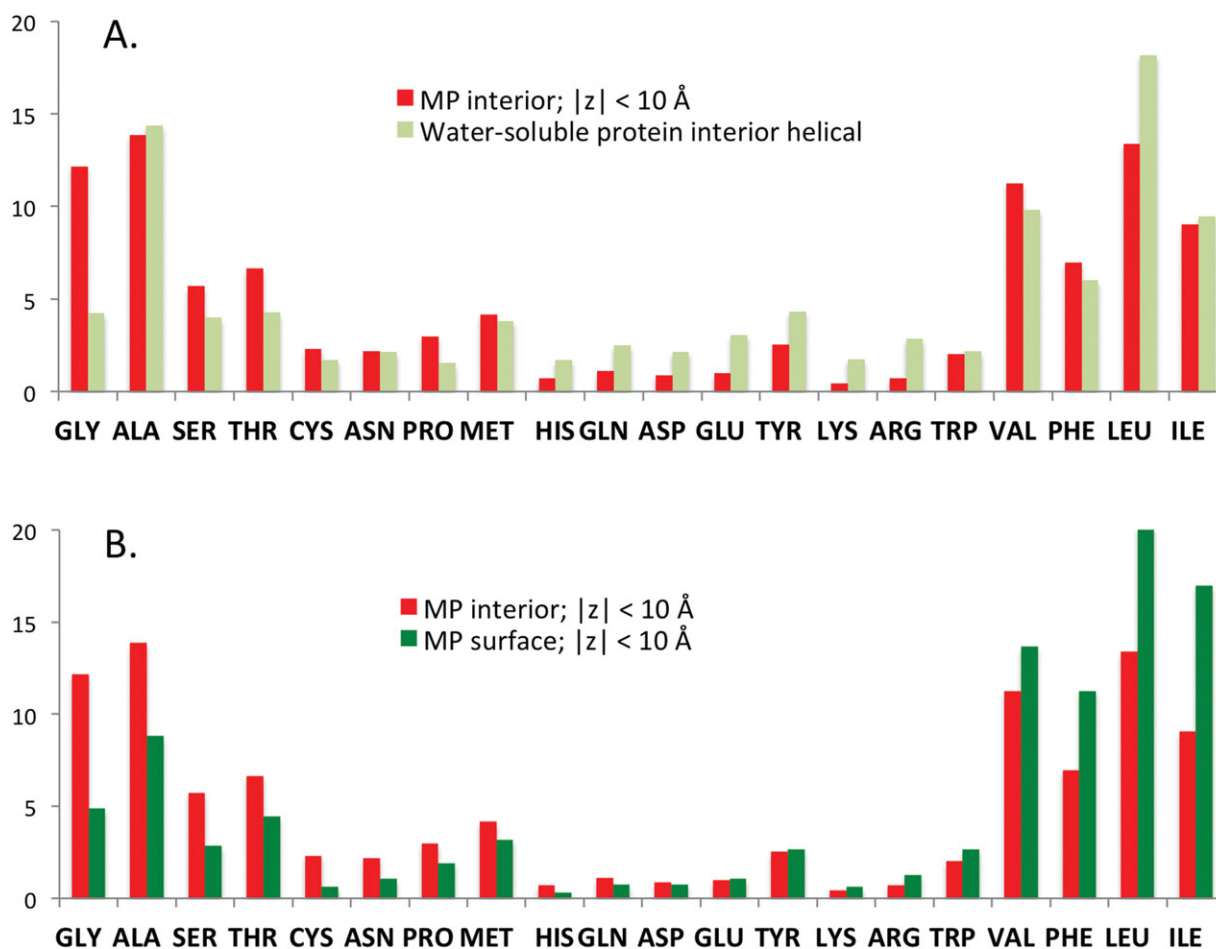


**Figure 1.** Amino acid compositions of helical membrane proteins and water-soluble proteins. For the membrane proteins, 26 structures assessed to be native-like<sup>3</sup> were used and only residues positioned in the membrane hydrophobic region (distance from membrane mid-plane  $< 10 \text{ \AA}$ ) were analyzed. For the water-soluble proteins, 2148 nonhomologous chains<sup>4</sup> were used and buried helical positions were analyzed. (A) Compositional difference in buried helical positions between the membrane proteins and water-soluble proteins. (B) Compositional difference between buried and surface positions in the membrane proteins. Amino acids are ordered according to the latter compositional difference.

hydrogen bonding capacity being largely satisfied by the helical structures, the scarcity of charged and large polar sidechains provides minimal opportunity for specific tertiary (and quaternary) interactions compared with water-soluble proteins [4.8% versus 14.0%, Fig. 1(A)]. However, the high abundance of Gly residues, and, to a lesser extent, Pro residues, in the TM helices provides unique opportunities for stabilizing tertiary (and quaternary) structures.<sup>5,6</sup> The use of Gly residues for tertiary and quaternary structural stability was recently reassessed.<sup>3</sup> In native-like TM domain structures, conserved Gly residues rarely face the lipid interstices, as doing so would expose the backbone polar groups; instead many of the Gly residues participate in close helix-helix packing. A comparison of the amino-acid compositions in the interior positions versus surface positions in the TM domains [Fig. 1(B)] shows that Gly, as well as amino acids with short nonpolar (i.e., Ala) and polar (i.e., Ser, Thr, and Asn) sidechains, favor interior positions over surface positions,

whereas amino acids with long nonpolar sidechains (i.e., Ile, Leu, and Phe) favor surface positions. This distribution clearly suggests that close packing of helices is of paramount importance for tertiary and quaternary structural stability, resulting in enhanced van der Waals interactions and backbone-backbone electrostatic interactions, such as C $\alpha$ H hydrogen bonding between helices.<sup>7</sup> Relative to the interior of water-soluble proteins, Gly in the internal positions of the native-like TM domains shows a threefold enrichment [Fig. 1(A)], clearly indicating the exceptional role of the smallest amino acid.

As Anfinsen recognized several decades ago, a protein structure results from the totality of interactions within the protein and between the protein and its environment.<sup>8</sup> There is no other class of proteins for which this statement is more important than for membrane proteins where the intraprotein interactions are weak and the interactions with the heterogeneous and anisotropic environment are substantial. Sanders has recently pointed out that the

lipid composition for a given membrane protein can vary significantly over the lifetime of the functional protein,<sup>9</sup> yet there are many biophysical properties of the membrane environment that remain largely unchanged despite variations in the lipid composition. For instance, the bilayer nature of the membrane, the hydrophobicity of the membrane interstices, and the hydrophobic thickness are to a very large extent invariant to the natural lipid composition that occurs during much of the life cycle of a typical cell. Synthetic lipid bilayers can model these biophysical properties well, whereas other membrane mimetics do less well. Detergent micelles have a monolayer structure, reduced hydrophobicity, and a malleable hydrophobic thickness, and thus do not constrain a TM helix to span the dimension of a native membrane.<sup>10</sup> Monomeric detergent molecules co-exist with detergent micelles at concentrations that are approximately 10<sup>6</sup>-fold greater than monomeric lipids that co-exist with lipid bilayers.<sup>11</sup> Such high concentrations of monomeric detergents can result in deformation of water-soluble regions of the protein or detergent penetration into the TM domain in a nonnative-like way. Detergents in a crystal lattice may or may not constrain the proteins in bilayer-like layers; often the hydrophobicity of the crystal lattice is weak and the hydrophobic thickness can be thin.<sup>12</sup> In such a high protein concentration environment, crystal contacts can significantly perturb the protein structure, especially since the tertiary and quaternary structure has relatively low stability. In short, the choice of membrane mimetics is important and structures determined in detergent-based mimetics especially need validation.

Solid-state NMR (ssNMR) spectroscopy is a tool for characterizing structures and dynamics of molecules that do not undergo isotropic motions on the NMR timescales. Consequently, this technique is appropriate for observing membrane proteins in lipid bilayers, either in liposomes via magic angle spinning (MAS) spectroscopy or in planar bilayers by oriented sample (OS) spectroscopy. MAS spectroscopy can yield torsion angle restraints from the isotropic chemical shifts of C', C $\alpha$ , and C $\beta$ , and short-range distances. In the TM domains of helical membrane proteins, interhelical distances between sidechains are difficult to obtain, because of the uniformity of the environment resulting in nearly identical frequencies for all the sidechain resonances of a given residue type (e.g., Leu). However, from anisotropic chemical shifts and dipolar interactions, OS spectroscopy can determine precise orientations of atomic sites in a protein relative to the bilayer normal. Such orientational restraints can be used to determine the tilt and rotation angles of each helix, thereby greatly reducing the need for interhelical distance restraints. Recently, it has been shown that orientational restraints can also be obtained from MAS

spectroscopy.<sup>13</sup> As a consequence of orientational restraints, sparse distance restraints obtained from the unique or rare residue types in the TM helices can provide the remaining necessary restraints for a high-resolution structural characterization.<sup>14–16,38</sup>

Here, we use the M2 protein from Influenza A virus as a model system to illustrate the challenges and techniques for gaining a native-like structure and a detailed functional understanding of a drug target. Like many viral proteins, the M2 protein has more than one function even though the amino-acid sequence is only 97 residues long (Fig. 2). The functional oligomeric state is a tetramer. It has long been known as a proton-selective channel<sup>21</sup> and as a protein that binds the M1 protein on the viral interior.<sup>20</sup> More recently its role in viral budding has become well documented.<sup>22,23</sup> The channel activity is associated with a single TM helix that as a tetramer forms a pore, which is interrupted by the H<sub>37</sub>xxxW<sub>41</sub> sequence in the C-terminal half of the TM helix (Fig. 2), a characteristic motif for Influenza proton channels.<sup>24</sup> It is the unique chemistry of this H<sub>37</sub>xxxW<sub>41</sub> quartet that accounts for acid activation, proton selectivity and gating of the channel. While the function of the N-terminal 22 amino acids is not well characterized, the C-terminal 35 amino acids are associated with binding the M1 protein. The structure for neither of these terminal segments are known for M2 from Influenza A (AM2), but the C-terminal segment of the Influenza B M2 protein (BM2), which has no sequence homology with the counterpart of AM2, has been characterized as well as a complex with the M1 protein.<sup>25</sup> Between the TM helix and the M1-binding segment of AM2 is an amphipathic helix (residues 47–62) that is located in the membrane inner interface and is important for viral budding.<sup>22,23</sup> It is thought that this amphipathic helix induces membrane curvature required for viral budding that arises from raft-like domains rich in cholesterol and sphingomyelin. The amphipathic helix appears to have a cholesterol recognition amino acid consensus (CRAC) motif<sup>26</sup> indicative of a cholesterol binding site, and Cys50 in the amphipathic helix is known to be palmitoylated (Fig. 2), a post-translational modification that is sometimes found to accompany cholesterol binding.<sup>27</sup> The combination of the TM and amphipathic helices, known as the conductance domain, in synthetic lipid bilayers appears to contain all of the residues and interactions with the environment necessary for achieving the detailed conductance properties of the native protein in oocytes.<sup>18</sup>

Along with the significant progress in experimental structural characterization, there have been important developments in computational modeling of the structure, dynamics, and gating mechanism of the M2 protein. In many ways M2 can be viewed as a success story in integrating experiment and

N term: MSLLETVETP<sub>10</sub> IRNEWGCRCN<sub>20</sub> DS  
 TM helix: SDPLVVAA<sub>30</sub> SIIGILHLIL<sub>40</sub> WILDRL  
 Amp Helix: FFKS<sub>50</sub> IYRFFEHLGLK<sub>60</sub> RG  
 C term: PSTEGVPE<sub>70</sub> SMREEYRKEQ<sub>80</sub>  
 QSAVDADDSH<sub>90</sub> FVSIELE<sub>97</sub>

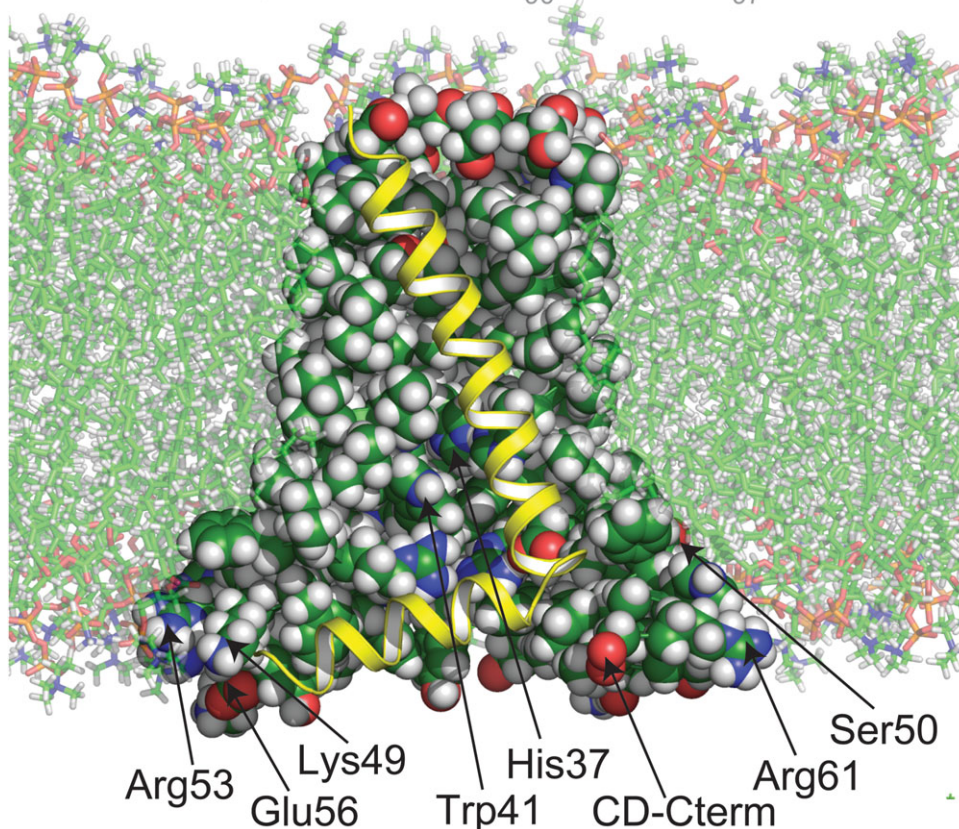


**Figure 2.** The amino acid sequence and functional domains of the C50S M2 protein from Influenza A virus. The N-terminal 22 amino acids have an unknown function, but could include tetramer stabilization via inter-chain disulfide bond formation of Cys17 and Cys19.<sup>17</sup> Amino acids 23–46 form a TM helix, with the signature H37xxxW41 motif located in the C-terminal half; amino acids 47–62 form an amphipathic helix. The TM and amphipathic helices, in the tetrameric form, produce the channel properties of the full-length protein.<sup>18</sup> The structure (2LOJ) of this conductance domain, characterized and refined in liquid crystalline lipid bilayers,<sup>19</sup> is shown in spacing-filling mode for the sidechains of three chains and as a yellow ribbon for the fourth chain. Some of the key residues are labeled. The C-terminal 35 amino acids bind the M1 protein.<sup>20</sup> [An interactive view is available in the electronic version of the article.](#)

computation for achieving detailed structural and functional understanding of a highly dynamic membrane protein.

### M2 Protein Structures

From more than a dozen structures of the Influenza A M2 protein using X-ray crystallography, solution and solid-state NMR spectroscopy as well as structural data from infrared spectroscopy, it is now possible to glean a considerable understanding of the influence of membrane mimetic environments on membrane protein structure.<sup>10,28</sup> An assortment of these structures is shown in Figure 3; Table I presents detailed information about the samples and

the methods of characterization as well as some key structural features. Despite the fact that these structures are not of the full-length protein, there has been considerable structural and functional validation of the constructs and of the use of synthetic lipid bilayers as models of the native membrane environment. As a result there are numerous important ramifications for the structures of helical membrane proteins determined in a wide range of detergent-based membrane mimetics that are being deposited in the Protein Data Bank (PDB).

Even before the first experimental structure for the M2 TM domain was determined, molecular modeling was used, in conjunction with experimental

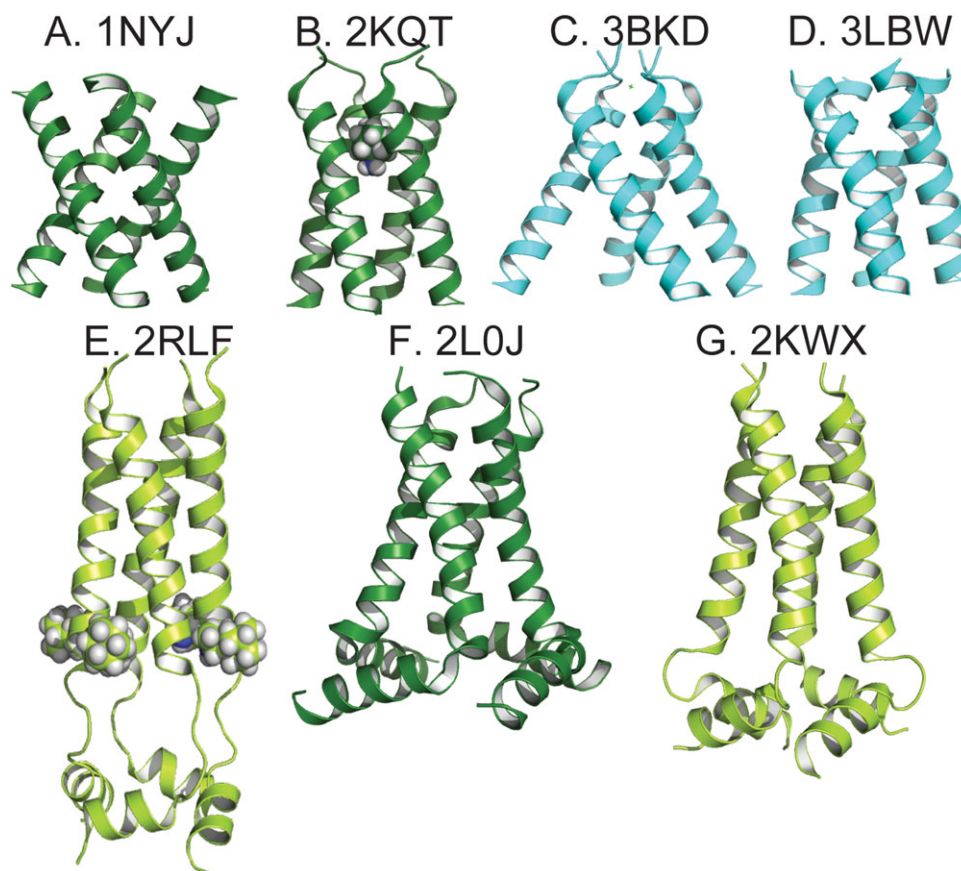


**Figure 3.** Structures of M2 protein constructs obtained by solid-state NMR spectroscopy in synthetic lipid bilayers, solution NMR spectroscopy in detergent micelles, and X-ray crystallography in detergent-based crystals. (A) 1NYJ. (B) 2KQT, with amantadine bound in the pore. (C) 3BKD. (D) 3LBW. (E) 2RLF, with each chain having a rimantadine molecule bound at an external site. (F) 2LOJ. (G) 2KWX. See Table 1 for additional information.

restraints (such as from cysteine scanning or site-directed infrared dichroism), to build structural models.<sup>29–32</sup>

The first M2 protein structures in the PDB were deposited in 2002 of the TM helix monomer and tetramer showing a left-handed helical bundle with Val27, Ser31, Gly34, His37, and Trp41 lining the pore [1MP6 and 1NYJ; Fig. 3(A)],<sup>33,34</sup> based on high-

resolution OS ssNMR spectroscopy of the polypeptide backbone in synthetic lipid bilayers. The helix tilt of 38° was greater than previously envisioned based on cross-linking studies<sup>35</sup> and molecular dynamics (MD) simulations.<sup>30</sup> However, the helix tilt and rotation angles of the four-fold symmetric helices were consistent with site-directed infrared dichroism results from a few labeled sites.<sup>32</sup> In 2007

**Table I.** Information for Various M2 protein Structures

PDB ID	Construct	Environment	pH	X-ray or NMR	Drug	Helix tilt angle (°) <sup>a</sup>
1NYJ	Ser22-Leu46	DMPC bilayer	7.0	ssNMR		38
2H95	Ser22-Leu46	DMPC bilayer	8.8	ssNMR	AMT in pore	30 N; 21 C
2KQT	Ser22-Leu46	DMPC bilayer	7.5	ssNMR	AMT in pore	32 N; 18 C
2LOJ	Ser22-Gly62 (C50S)	DOPC/DOPE bilayer	7.5	ssNMR		32 N; 22 C
3BKD	Ser22-Leu46 (I33SeM)	OG/PEG bilayer-like	7.3	X-ray (2.05 Å)		33
3C9J	Ser22-Leu46 (G34A)	OG/PEG bilayer-like	5.3	X-ray (3.5 Å)	AMT in pore	36
3LBW	Pro25-Leu46 (G34A)	OG/PEG bilayer-like	6.5	X-ray (1.65 Å)		32 N; 17 C
2RLF	Arg18-Lys60 (C50S)	DHPC micelles	7.5	solution NMR	RMT in ext site	16
2KWX	Arg18-Lys60 (V27A, C50S)	DHPC micelles	7.5	solution NMR		15

<sup>a</sup> Tilt angles were calculated using residues 23 to 46 for the TM helix or using residues 23 to 32 and 35 to 46 separately for the N-terminal and C-terminal halves when a kink near Gly34 is apparent. Fewer residues were used when terminal residues were either missing or not helical; these exceptions were: 2H95, starting at residue 24 and ending at residue 43; and 2KQT and 3C9J, both starting at residue 24; 2H95 and 3LBW each had two residues added at the N-terminus, by modeling after 2KQT and 2LOJ, respectively. SeM, selenomethionine; OG, octylglucoside; PEG, polyethylene glycol; AMT, amantadine; RMT, rimantadine.

the structure of the same construct in the presence of the antiviral drug amantadine was published (2H95).<sup>36</sup> The primary structural influence of drug binding was to induce a kink in the TM helix just below what was presumed to be the binding site, Gly34. The kink had only a small effect on the tilt of the N-terminal portion of the helix, but reduced the tilt of the C-terminal portion to 21°.

Since the early computational efforts in model building, both the parameterization for explicit representation of lipid molecules in molecular mechanics force fields and our ability to carry out MD simulations in an explicit membrane have improved significantly. A fruit borne of the ever more realistic representation of the lipid environment was seen in a 2008 study.<sup>37</sup> In the MD simulations of the M2 TM domain starting from both the 2002 ssNMR structure in the absence of a drug molecule [1NYJ; Fig. 3(A)]<sup>34</sup> and the 2007 ssNMR structure in the presence of amantadine (2H95),<sup>36</sup> the packing of the helix bundle tightened, resulting in a distinct reduction in the pore size, in line with the more recent ssNMR and X-ray crystal structures [Fig. 3(D,F)]. Moreover, the Val27 sidechains were found to extend into the pore to form a constriction, leading to the proposition of a secondary gate.<sup>37</sup> This secondary-gate configuration of Val27 has been confirmed in all recent structures.

The 2007 TM domain structure in the presence of amantadine was later refined by Cady *et al.* with MAS ssNMR-derived distance measurements between helices as well as between the helices and the drug, positioning the drug in the pore [2KQT; Fig. 3(B)].<sup>38</sup> In 2010 the structure of the M2 conductance domain was characterized by OS ssNMR and refined by restrained MD simulations in the same explicit lipid bilayer (2L0J; Fig. 2).<sup>19</sup> The TM helical bundle was more tightly packed than in the original 2002 structure [Fig. 3(A,F)]. The amphipathic helices were positioned in the membrane interface with the hydrophobic residues facing into the lipid hydrophobic region and the numerous charged residues (dominated by lysine and arginine residues) interacting with the lipid headgroups (Fig. 2). Furthermore, the Ser50 residue (replacing the native Cys50) is positioned so that its hydroxyl is at a level in the bilayer consistent with the glycerol backbone of the lipids, an appropriate position for palmitylation.

In 2008 the first X-ray crystal structures of the M2 TM helices were solved, showing a tetrameric left-handed bundle (consistent with the ssNMR structures) both in the absence [3BKD; Fig. 3(C)] and presence of amantadine (3C9J).<sup>39</sup> The latter structure also bore a stabilizing mutation, G34A. However, both structures appeared to be significantly perturbed by the membrane mimetic environment, as evidenced by the severe splaying of the TM

helices and, in the case of 3BKD, the presence of octylglucoside and polyethylene glycol in the pore and the interhelical interface. The same G34A mutant at a slightly lower pH without drug was characterized in 2010 [3LBW; Fig. 3(D)],<sup>40</sup> presenting a better packed tetrameric structure, with no detergent in the pore or interhelical interface. The backbone structure of 3LBW is very similar to the TM helical bundle of 2L0J characterized in lipid bilayers (C $\alpha$  RMSD of 0.6 Å for P25-W41), but the H<sub>37</sub>xxxW<sub>41</sub> sidechain conformations are different (Fig. 4).

Also in 2008 the first solution NMR structure of M2 was determined in DHPC micelles, providing the first structure of the conductance domain [2RLF; Fig. 3(E)].<sup>42</sup> This structure had the surprising result that the antiviral drug rimantadine did not bind in the pore but to an external site on each chain of the tetramer, facing what would be the viral membrane inner interfacial region. Moreover, the amphipathic helix was not positioned in the membrane interface [Fig. 3(E,F)], but formed a separate water-soluble four-helix bundle that was completely H/D exchangeable. The latter observation was in contrast to H/D exchange results from the full-length protein in lipid bilayers.<sup>43</sup> As noted above, in the 2KQT structure refined by Cady *et al.* from 2H95, the pore was identified as the primary drug binding site [Fig. 3(B)].<sup>38</sup> The external drug-binding site appeared to be in conflict with a variety of studies, including stoichiometry experiments,<sup>44</sup> but with the 2010 ssNMR structure for the conductance domain (2L0J) it was realized that, when the amphipathic helix binds to the membrane interface, the potential drug binding site suggested by the solution NMR structure becomes occluded by two hydrophobic amino acids.<sup>19</sup> Also in 2010 a drug resistant mutant (V27A) of the conductance domain was characterized in the same DHPC micelles [2KWX; Fig. 3(G)].<sup>45</sup> This time the amphipathic helix was found to bind in the micellar interfacial region. In 2011 Pielak *et al.* came around with a rimantadine-bound structure of an AM2-BM2 chimera for the TM domain, showing the drug in the pore (2LJC).<sup>46</sup> The controversy regarding the drug binding site now seems firmly settled on the pore site.

Amphipathic helices that interact with the lipid interfacial region take advantage of the steep dielectric and water concentration gradients between the hydrophobic core and lipid headgroup region. This is also where the largest feature of the lateral pressure profile is located.<sup>47</sup> In detergent micelles these gradients and the lateral pressure profile are much weaker. In addition, the curvature of the monolayer surface may further influence the propensity of amphipathic helices to interact with the detergent interfacial region. Apparently, for the M2 conductance domain the interaction of the amphipathic

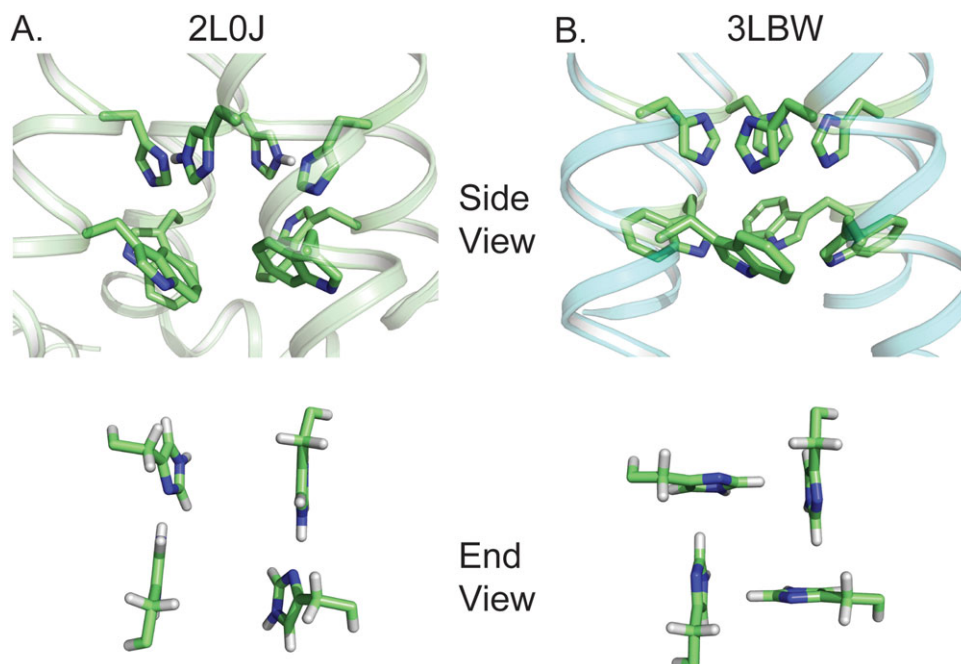


**Figure 4.** Conformations of the H<sub>37xxx</sub>W<sub>41</sub> quartet in the ssNMR structure 2LOJ<sup>19</sup> and X-ray structure 3LBW,<sup>40</sup> shown in both side and top views. (A) The dimer of dimers conformation in 2LOJ was refined by QM/MM calculations based on significantly downfield-shifted imidazolium <sup>15</sup>Nδ1 and <sup>15</sup>Nε2 resonances, obtained in lipid bilayers, that indicated strong imidazole-imidazolium hydrogen bonds at pH 7.5.<sup>41</sup> (B) The fourfold symmetric conformation in 3LBW was from the TM domain in an octylglucoside and polyethylene glycol preparation at pH 6.5. Both structures show the Trp41 residues forming a basket as a gate for proton conductance. [An interactive view is available in the electronic version of the article.](#)

helices with the lipid environment is much stronger than with the DHPC micelle, where these helices form a water soluble bundle as in 2RLF [Fig. 3(E)].<sup>42</sup> On the other hand, the solution NMR structure of the V27A mutant [2KWX; Fig. 3(G)] had the amphipathic helices interacting with the detergent interfacial region, with the same helix rotation, but somewhat different helix tilt, lateral position, and depth compared with the structure obtained in the bilayer environment [2LOJ; Fig. 3(F)]. Potentially, this helix has different preferred orientations when it is in the mature virion (conducting protons) and when it is facilitating viral budding by inducing bilayer curvature.

It now seems clear that the TM helices form a tetrameric structure similar to the 2002 structure (1NYJ; Fig. 3(A)), but with somewhat tighter packing and somewhat smaller tilt angles for the helices relative to the pore axis (32° for the N-terminal half; Table I), as visualized in the recent ssNMR and X-ray structures [2LOJ and 3LBW; Fig. 3(F,D)]. In both of the solution NMR structures (2RLF and 2KWX; Fig. 3(E,G)), the TM helices in DHPC micelles have much smaller tilt angles (16° and 15°, respectively) relative to the pore axis. The result is that the secondary gate formed by the Val27 residues, first identified through MD simulations,<sup>37</sup> appears to be more tightly shut than when the helices are tilted at a 32° angle as in 2LOJ and 3LBW.

In the native membrane the protein and membrane environment are likely to be mutually involved in determining the hydrophobic dimension of the protein. Detergent micelles are much more adaptable to the hydrophobic dimension presented by the membrane protein than a lipid bilayer. Consequently, while amantadine and rimantadine bind to M2 in the pore when it is in the virion, these drugs do not bind to WT M2 in the pore when it is in DHPC micelles (as in 2RLF), potentially because of the small helix tilt angles that close the secondary gate too tightly for the drug to enter.

Interestingly, these structural results showing different tilts for the M2 TM helices are not a reflection of the structural precision for the X-ray, solution or ssNMR structures. Although the 3C9J crystal structure has only 3.5 Å resolution, the 3BKD structure is high resolution at 2.05 Å. The 3LBW structure is even better at 1.65 Å, but the 7.4 Å RMSD between the latter two structures does not reflect this enhancement in resolution. Similarly, the resolution of the solution NMR structures is good enough to define the tilt for M2 TM helices in the NMR sample, and via the orientational restraints of OS ssNMR there is accuracy within 2° in the characterization of helix tilt even in liquid crystalline lipid bilayers.<sup>2</sup> This emphasizes the need for membrane mimetics that are similar to the native membrane in restraining the membrane protein structure. So although the

orientational restraints from ssNMR do not define all of the sidechain conformations in the TM helices, the precision in determining the tilt of the helices is equivalent to the precision in a high-resolution X-ray structure, but with the sample for the ssNMR structure in a native-like bilayer environment. Of course, detergent-based crystals can also produce native-like structures, as in 3LBW [Fig. 3(D)].

Over the years considerable MAS spectral results have been published supporting the TM helical structure, amantadine binding site, and confirming which residues are facing the pore.<sup>48,49</sup> In 2012 the <sup>13</sup>C MAS resonances of the TM helix of the conductance domain were substantially assigned and multiple distance restraints observed, confirming the 2010 ssNMR structure 2LOJ.<sup>14</sup> In addition, the first MAS spectra of the full-length M2 protein have been obtained,<sup>15</sup> showing that the conformations of the TM helices are the same in the conductance domain and in the full-length protein. In addition, MAS spectra of the full-length protein directly observed in *Escherichia coli* membranes has been obtained where the protein was inserted into the membrane via the cellular machinery and was never exposed to detergents. Once again the spectra were the same as that observed for the full-length protein that had been isolated from *E. coli*, purified in detergents and reconstituted into synthetic lipids. This provided excellent validation for the structure obtained in synthetic lipid bilayers.

### Drug Binding Kinetics and Drug-Resistant Mutations

Amantadine and rimantadine have been on the market as anti-flu pharmaceuticals for decades until recently, when the seasonal flu and the recent swine flu pandemic presented M2 as the S31N drug resistant strain. The binding rate constant of amantadine for the wild-type M2 is  $600 \text{ M}^{-1} \text{ s}^{-1}$ , much lower than the diffusion-controlled limit, but, with an unbinding rate constant of  $3 \times 10^{-4} \text{ s}^{-1}$ , the binding is practically irreversible.<sup>50,51</sup> The latter property makes these compounds effective pharmaceuticals. Consequently, a modest impairment to the drug-binding site by further reducing the on-rate or a significant opening of the secondary gate that increases the off-rate will defeat the effectiveness of these pharmaceuticals. A reduction of the helix tilt in DHPC micelles accomplishes the former and drug resistance of the V27A mutant may be due to the latter effect. Recently, Hong *et al.* have reported that the M2 tetramer does not bind drugs while in lipid bilayers mimicking the bulk viral coat, that is, bilayers high in cholesterol and sphingomyelin.<sup>52</sup> Such bilayers have a significantly greater hydrophobic thickness than the liquid crystalline plasma membrane. It is reasonable to assume that the helix tilt would be reduced in such an environment, thereby influencing

the on-rate in much the same way that the DHPC micelle environment has resulted in smaller helix tilt angles and a lack of drug binding.

The last observation suggests that this viral-coat mimetic may not be a good model of the native M2 environment. In fact, it was recently discovered that M2 is localized at the neck of the budding virus, where the raft-like domains of the nascent virion meet the remaining bulk plasma membrane.<sup>22,23</sup> M2 in the lower-cholesterol environment of the plasma membrane alters the membrane curvature, via the amphipathic helix, and thereby facilitates membrane scission and release of the budding virus. After release, a significant fraction of the M2 tetramers are expected to stay in the lower-cholesterol membrane environment as part of the virion. Fortunately for further viral replication, only a small number of protons are needed to acidify the viral interior upon endocytosis and consequently, a relatively small number of M2 proton channels are required to be in the liquid crystalline bilayer environment of the virion for adequate proton conductance. It is also the latter environment that sustains the known drug binding properties of M2.

Before structural information was available regarding the drug-binding site, it was widely assumed that the drugs bind in the channel pore, given that drug-resistant mutations (e.g., V27A, A30T, and S31N) occurred in likely pore-lining positions. Amantadine was modeled into the pore and MD simulations were used to better define the interactions of the bound drug with the protein residues. One simulation study placed the amantadine binding site near Ala29.<sup>53</sup> A subsequent study found amantadine to be surrounded by the sidechains of Ala30 and Ser31 with the bound drug molecule and the Val27 secondary gate forming an extended blockage of the channel pore.<sup>37</sup> In a third simulation study, the drug molecule is slightly moved toward the C-terminal side.<sup>54</sup> These simulation results provide a rationalization for the drug-resistant mutations. In particular, the extended blockage formed by the bound drug molecule and Val27 lends credence to the earlier suggestion that the V27A mutation may cause drug resistance by eliminating the secondary gate and increasing the off-rate (though not necessarily affecting the binding affinity<sup>55</sup>).

With the brief controversy regarding possible external drug binding sites now settled, the M2 protein has received renewed interest as a drug target.<sup>56</sup> Computation has been useful in identifying compounds that are potent inhibitors of the V27A mutant.<sup>57</sup> However, no effective inhibitor of the most common M2 mutant, S31N, has been found.<sup>[\*]</sup>

\*Recently, DeGrado and coworkers have published the first inhibitors for the M2 S31N mutant in PNAS 110:1315-1320 (Wang *et al.*, 2013).

### Characterization of the H<sub>37</sub>xxxW<sub>41</sub> Quartet

The heart of the M2 proton conductance capability is in the H<sub>37</sub>xxxW<sub>41</sub> sequence that is the signature motif for Influenza proton channels (Fig. 4).<sup>24</sup> The pK<sub>a</sub>s of the histidines were first characterized by Hu *et al.*,<sup>41</sup> with the surprising finding that two of the His37 residues of this tetrad in the middle of the bilayer environment had higher affinity for protons than His residues on the surface of water soluble proteins. These two high proton-affinity pK<sub>a</sub> values for the M2 tetramer were both 8.2. In comparison, the His37 residue in the M2 monomeric TM helix in detergent micelles is about 1.5 pH units lower, at 6.8.<sup>58</sup> The latter value is similar to that of a water-exposed histidine.

The identical value of the first two pK<sub>a</sub>s of the M2 histidine tetrad further suggests cooperative proton binding. That is, the first protonation results in a structural change that facilitates the second protonation. It is known that M2 becomes activated at a pH of approximately 6.5.<sup>59</sup> The third pK<sub>a</sub> for the histidine tetrad determined in the bilayer environment was approximately 6.3,<sup>41</sup> consistent with this third proton being the charge responsible for activating the proton channel. A fourth pK<sub>a</sub> was suggested in this study to be below pH 5.

Because of the linkage between proton binding and tetramerization,<sup>[†]</sup> a higher proton binding affinity in the tetramer than in the monomer necessarily means that the tetramer stability increases upon binding the proton. Therefore, from the set of His37 pK<sub>a</sub>s one can conclude that the tetramer stability increases as the pH is lowered from 9.0 to ~6.5 and then decreases as the pH is further lowered. This is exactly what was observed by Ma *et al.*,<sup>18</sup> the pH dependence of the tetramer stability calculated from the set of observed His37 pK<sub>a</sub>s was in quantitative agreement with their measurement. As noted by Ma *et al.*, it might seem counterintuitive that placing two charges in close proximity (within ~6 Å) in a low dielectric environment should increase the stability of the tetramer. Based on the appearance of imidazolium <sup>15</sup>Nδ1 and <sup>15</sup>Nε2 resonances that are significantly downfield-shifted, similar to model imidazole-imidazolium spectra,<sup>60</sup> Hu *et al.*<sup>41</sup> proposed that the His37 residues formed a pair of imidazole-imidazolium hydrogen bonded dimers, which would significantly enhance tetramer stability.<sup>19</sup> In addition, the strong hydrogen bonds could disperse each charge over two rings, thereby reducing the charge-charge repulsion that could be anticipated. The exchange broadening of the resonances suggests His37 sidechain dynamics (see below).

<sup>†</sup>Linkage is a term introduced by Wyman to mean that, if a ligand has different affinities for two states (in the present case monomer and tetramer), then ligand binding will push the equilibrium between the two states toward the one with high ligand affinity.

Recently, a new set of pK<sub>a</sub>s were determined for the M2 TM domain by Hu *et al.* in the high sphingomyelin/cholesterol environment.<sup>61</sup> The highest pK<sub>a</sub> was 7.5, the second was 6.8 and the third 4.9. These values suggest a substantially reduced affinity for protons, but also a lack of cooperative proton binding and consequently the loss of imidazole-imidazolium hydrogen bonding that stabilizes the tetramer. As noted above, the high sphingomyelin/cholesterol content results in a substantial increase in the bilayer hydrophobic thickness, and is therefore expect to alter the helix tilt. The sensitivity of the TM domain tetramer structure to hydrophobic thickness has been experimentally demonstrated using a variety of lipid chain lengths.<sup>62</sup> In addition to altering the drug binding affinity, a smaller helix tilt would change the geometry of the histidine tetrad by altering the orientation of the backbone with respect to the bilayer normal. The formation of the imidazole-imidazolium hydrogen bonds is highly sensitive to the orientation of the His37 Cα-Cβ bonds. Consequently, the new set of pK<sub>a</sub>s appears to reflect influences by the lipid environment.

We argue here that these pK<sub>a</sub>s are not associated with the proton channel function of the M2 protein, although this is a matter of debate.<sup>63</sup> At issue is whether M2 functions in a low-cholesterol, liquid-crystalline environment or in a high sphingomyelin/cholesterol environment. Several lines of evidence suggest the former scenario. First, as described above, for viral budding, M2 is needed at the periphery of raft-like domains, that is, in a small region of low-cholesterol, liquid-crystalline plasma membrane that would be pinched off and integrated into the virion upon its release. Second, extraction by Triton X-100 of M2 in virus-infected cell membranes<sup>64</sup> and in synthetic membranes<sup>65</sup> showed that most of the M2 protein is not associated with raft-like domains. Third, although M2 is expressed at nearly the same level as hemagglutinin and neuraminidase, the occurrence of M2 in the virion is substantially under-represented compared with the other two proteins that reside in the raft-like domains.<sup>66</sup> That the under representation reflects exclusion of M2 from raft-like domains is supported by the observation that the M2 to hemagglutinin and neuraminidase ratios increased when the fraction of non-raft-related lipids increased in the membranes,<sup>64</sup> as well as the fact M2 has a significantly shorter transmembrane hydrophobic sequence than the other two proteins (19 amino acids vs. 26–28 amino acids). Fourth, any M2 tetramer present in a raft-like domain should be ineffective for proton conductance. As already pointed out, the protein does not bind amantadine in the raft-like lipids and consequently, if wild-type M2 were to conduct protons in this environment then amantadine would be a completely ineffective drug, which we know from decades of

pharmacological use not to be the case. Therefore, we contend that M2 requires a low-cholesterol lipid environment for virus budding, drug binding, and proton conductance. This liquid-crystalline environment allows M2 to bind protons cooperatively and with high affinity.

Until recently the dimer (or pair) of dimers symmetry appeared to be associated with just the His37 sidechain. Andreas *et al.* showed in 2010 that this symmetry also extended to multiple backbone sites in studies of the conductance domain by MAS spectroscopy in POPC bilayers above the gel to liquid crystalline phase transition temperature.<sup>67</sup> They also observed a similar doubling of specific backbone resonances of the conductance domain in DPhPC bilayers. We confirmed these results in MAS spectra of DOPC bilayer preparations below the phase transition temperature.<sup>14</sup> A model for the subtle conformational difference originating at His37 has been suggested by Sharma *et al.* (Fig. 5).<sup>19</sup> The C $\alpha$ -C $\alpha$  separation in an imidazole-imidazolium dimer appears to be slightly larger than the C $\alpha$ -C $\alpha$  separation between His37 residues in different dimers. That is, in a pair of dimers configuration, the four His37 C $\alpha$  atoms form a rectangle with short distances between the dimers and longer distances within the dimers. Since the dimers appear to interconvert slowly based on the exchange broadening observed in the His37 titration,<sup>41</sup> this could explain the MAS spectra showing that the dimer of dimers symmetry extends throughout much of the TM domain.

The characterization of the sidechain geometry of the H<sub>37</sub>xxxW<sub>41</sub> quartet and surrounding sidechains is complicated by dynamics described above and the dynamics associated with proton activation and conductance that will modulate interatomic distances. Observed distances should be interpreted in light of these motions and yet these pH dependent motions have not been well characterized by ssNMR. At temperatures below the phase transition, heterogeneity may replace the dynamics.

In such a situation involving large amplitude dynamics, distance restraint weighted conformational averages observed in solution NMR may not be particularly meaningful for determining the His37 sidechain conformation. Consequently, these sidechain conformations have not been extensively interpreted in the solution NMR structures. The early crystal structure appears to be perturbed, as an octylglucoside forms a hydrogen bond with His37. On the other hand, the recent crystal structure (3LBW) shows a four-fold symmetric structure even for the His37 sidechain and even though the sample was prepared at pH 6.5. Consequently, this structure presumably with two or three charges on the histidine tetrad does not provide an explanation for the cooperativity in proton binding, the enhanced stability of the tetramer at pH 6.5 nor the exchange broadening of the His37 resonances. Clearly, much

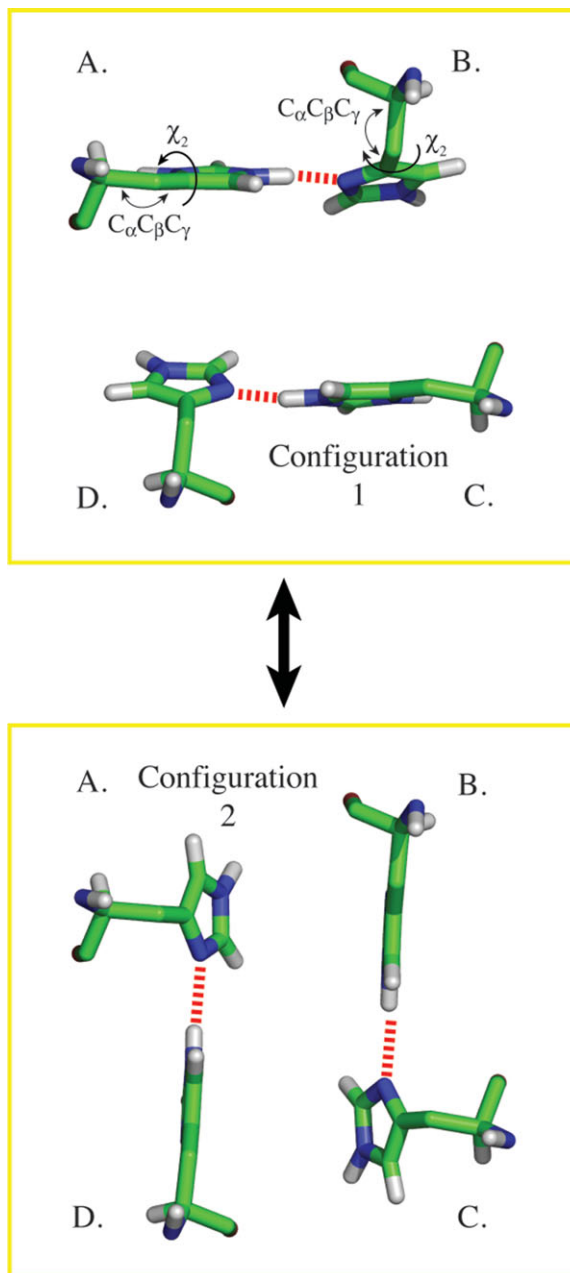


**Figure 5.** Exchange of partners between the two imidazole-imidazolium dimers, adapted from Sharma *et al.*<sup>19</sup> In the top panel, dimers are formed between chains A and B and between chains C and D; the bottom panel models the configuration with AD and BC dimers. The conversion between the two configurations can be accomplished by 90° changes in  $\chi_2$  and 10° changes in C $\alpha$ -C $\beta$ -C $\gamma$  angles (so that strained C $\alpha$ -C $\beta$ -C $\gamma$  angles become relaxed and vice versa), and is facilitated by proton exchange with nearby water molecules. [An interactive view is available in the electronic version of the article.](#)

more work is needed to characterize not only the dynamics, but also the pH-dependent conformational states of the H<sub>37</sub>xxxW<sub>41</sub> quartet so that the functional mechanism of M2 can be refined.

The gating mechanism has attracted particular attention for computational studies over the years. An early favored model posits that protonation of His37 residues leads to their repulsion, creating an open pore with a continuous water wire for proton conduction.<sup>30,53,68,69</sup> The proton conductance calculated from such a model was 53 pS, or  $3 \times 10^8$  protons per second. However, conductance measurements, especially more recent ones using liposome preparations, place the conductance at the level of  $\sim 3 \times 10^2$  protons per second.<sup>19,70–74</sup> The six orders of magnitude discrepancy casts doubt on this gating model.

An alternative model was proposed by Pinto *et al.*,<sup>31</sup> in which the His37 tetrad relays the proton from one side of the membrane to another. Quantum mechanics/molecular mechanics (QM/MM) calculations on the H<sub>37</sub>xxxW<sub>41</sub> quartet, constrained by the backbone structure of 2LOJ, were carried out to investigate the plausibility and provide atomic details of this model.<sup>19</sup> These calculations first confirmed that the doubly protonated His37 tetrad can form a stable dimer of dimers configuration (Fig. 5). Interestingly, unlike imidazole-imidazolium crystals, where the two imidazole rings sharing a proton are perpendicular to each other, the two His37 side-chains forming a dimer within the confines of the backbone structure are nearly coplanar. This dimer arrangement is stabilized in part by a hydrogen bond between N $\delta$ 1 and the backbone carbonyl, formed at the expense of an enlarged C $\alpha$ -C $\beta$ -C $\gamma$  angle (by  $\sim 10^\circ$ ; Fig. 5). The stable dimer of dimers configuration thus forms a barrier for proton conductance.

The QM/MM calculations further showed that a dimer can receive a proton from a hydronium ion from the N-terminal side of the pore, and pass it onto a water molecule on the C-terminal side of the pore via a  $45^\circ$  change in the His37  $\chi_2$  torsion angle and relaxation of the His37 C $\alpha$ -C $\beta$ -C $\gamma$  angle if the Trp41 primary gate is open. Hence, the His37 side-chains do not need to undergo dramatic rotations during the proton relay. On the other hand, the motion of the Trp41 primary gate could be coupled to the motion of the backbone. In line with the conformational change upon binding amantadine,<sup>36</sup> MD simulations<sup>75</sup> have shown that the TM helix can bend in the vicinity of Gly34, leading to fluctuations in the size of the C-terminal pore. In the backbone conformations with a larger pore, the Trp41 indoles prefer to orient parallel to the pore axis, exposing the His37 tetrad to the aqueous environment of the viral interior.

Alternatively, based on the ssNMR structure 1NYJ, which was determined at pH 7.0, and the X-ray crystal structure 3C9J determined at pH 5, Klein, Khurana *et al.* proposed a transporter-like model for backbone conformational transitions.<sup>76</sup>

According to this model, the 1NYJ structure, with the His37 tetrad presumably in the doubly-protonated state and a wide N-terminal pore entrance, represents the state poised for accepting a proton from the N-terminal side; the 3C9J structure (or a model built from it), with the His37 tetrad presumably in the triply-protonated state and a wide C-terminal pore entrance, represents the state in which a proton has been taken up and is ready for release to the C-terminal side. However, as noted above, the N-terminal pore entrance in 1NYJ is likely to be too wide (due to lack of interhelical distance restraints) and is tightened during MD simulations in explicit membrane.<sup>37</sup> The wide C-terminal pore entrance in 3C9J could be due to perturbation by the crystal environment.

The proton relay mechanism delineated by Sharma *et al.*<sup>19</sup> was further developed into a mathematical model for calculating proton conductance.<sup>77</sup> Coming from either side of the membrane, proton binding to the His37 tetrad was modeled as a diffusion-controlled reaction. Once bound, the proton can be released to either side of the membrane; the binding and unbinding rate constants are constrained by the third pK<sub>a</sub> ( $\sim 6.3$ ) of the His37 tetrad. In addition, the dynamics of the primary and secondary gates affect the transport of protons into the pore, and this was modeled into the calculations of the binding rate constants. This model<sup>78</sup> predicts proton conductance in the observed range (i.e., up to  $3 \times 10^2$  protons per second) and quantitatively reproduces observed current–voltage and current–pH relations<sup>19,79,80</sup> [Fig. 6(A)]. Moreover, it reproduces a 2-fold decrease in current when the solvent is changed from H<sub>2</sub>O to D<sub>2</sub>O,<sup>81</sup> observed by Mould *et al.*<sup>70</sup> [Fig. 6(B)].

## Conclusion

Theoretical and computational modeling has become an integral part of structural biology. Perhaps, this is particularly true in dealing with the subtle stability of small helical membrane proteins. In M2 the addition of two positive charges into the low dielectric interior of the TM domain appeared to be incongruous with enhanced stability of the tetramer. However, through QM/MM calculations hydrogen bonds between the imidazole rings and to the polypeptide backbone explain the enhanced stability of this charged state. The theoretical modeling of proton conductance leads to validation of the structure and to a much deeper understanding of the conductance mechanism.

Within the TM domain of the M2 protein from Influenza A virus, in addition to a pair of inter-histidine hydrogen bonds that can form near neutral pH, contributions to tetramer stability largely come from van der Waals interactions between the TM helices. Clearly, the membrane mimetic environment can have significant influences on the structure and

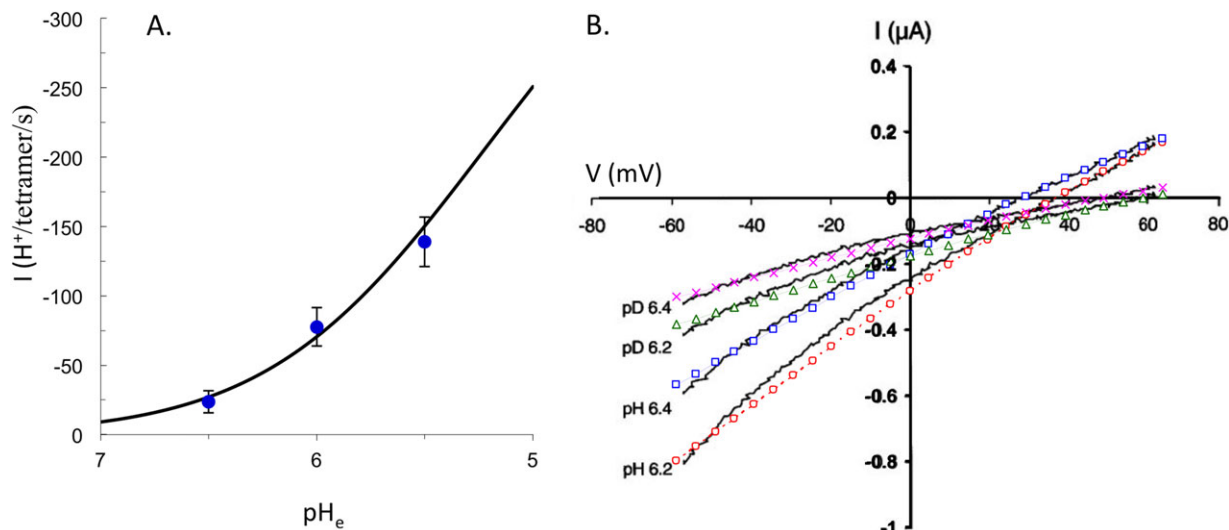


**Figure 6.** Comparison of calculated and experimental results for the M2 proton transport rate. (A) Dependence on pH, taken from Zhou.<sup>78</sup> Experimental results, shown as symbols, are from Sharma *et al.*<sup>19</sup> (B) Solvent isotope effect, taken from Zhou.<sup>81</sup> Experimental results, shown as continuous curves, are from Mould *et al.*<sup>70</sup>

function of the TM domain. In particular, the helix tilt is sensitive to the hydrophobic dimension of the environment. The solution NMR structures in detergent micelles appear to have helix tilt angles that are too small to support amantadine binding in the pore. Detergents have a dramatically higher monomeric concentration than lipids and hence individual detergent molecules can become embedded within the protein structure as in the early crystal structure. However, a more recent crystal structure (3LBW) of a stabilizing mutant has a very similar backbone structure to that obtained for the wild type protein by ssNMR in liquid crystalline lipid bilayers (2LOJ). Nevertheless the subtle details of the histidine tetrad essential for proton conductance appear to be lost in the 3LBW crystal structure.

The thick hydrophobic raft-like environment with high concentrations of sphingomyelin and cholesterol typical of the bulk viral coat does not support an M2 conformation consistent with the functional properties of the native protein. Neither the binding of amantadine nor the cooperative binding of protons that leads to the enhanced tetramer stability of the protein is observed in this environment. Surprisingly the incompatibility of the raft-like environment with proton conductance and drug binding augurs well for another function of the M2 protein, that of viral budding, which requires the positioning of M2 in the boundary between the raft-like environment and the bulk plasma membrane for the pinching off of the viral particle.

M2 has been an important proving ground for understanding the balance of intra-protein interactions and the interactions between a protein and its environment. The strategy of combining structural data obtained from native-like environments with

computational and theoretical modeling to unearth functional mechanisms, illustrated here, should have wide applications.

## References

- Eilers M, Patel AB, Liu W, Smith SO (2002) Comparison of helix interactions in membrane and soluble alpha-bundle proteins. *Biophys J* 82:2720–2736.
- Page RC, Kim S, Cross TA (2008) Transmembrane helix uniformity examined by spectral mapping of torsion angles. *Structure* 16:787–797.
- Dong H, Sharma M, Zhou HX, Cross TA (2012) Glycines: role in alpha-helical membrane protein structures and a potential indicator of native conformation. *Biochemistry* 51:4779–4789.
- Chen H, Zhou HX (2005) Prediction of solvent accessibility and sites of deleterious mutations from protein sequence. *Nucleic Acids Res* 33:3193–3199.
- Javadpour MM, Eilers M, Groesbeek M, Smith SO (1999) Helix packing in polytopic membrane proteins: role of glycine in transmembrane helix association. *Biophys J* 77:1609–1618.
- Russ WP, Engelman DM (2000) The GxxxG motif: a framework for transmembrane helix-helix association. *J Mol Biol* 296:911–919.
- Senes A, Ubarretxena-Belandia I, Engelman DM (2001) The  $\alpha$ ---H...O hydrogen bond: a determinant of stability and specificity in transmembrane helix interactions. *Proc Natl Acad Sci USA* 98:9056–9061.
- Anfinsen CB (1973) Principles that govern the folding of protein chains. *Science* 181:223–230.
- Sanders CR, Mittendorf KF (2011) Tolerance to changes in membrane lipid composition as a selected trait of membrane proteins. *Biochemistry* 50:7858–7867.
- Cross TA, Sharma M, Yi M, Zhou HX (2011) Influence of solubilizing environments on membrane protein structures. *Trends Biochem Sci* 36:117–125.
- Cevc G, Marsh D. 1987. Phospholipid bilayers: physical principles and models. New York: John Wiley & Sons.

12. Zhou HX, Cross TA (2013) Influences of membrane mimetic environments on membrane protein structures. *Annu Rev Biophys* 42.
13. Das B, Nothnagel H, Lu G, Son WS, Tian Y, Marassi FM, Opella SJ (2012) Structure determination of a membrane protein in proteoliposomes. *J Am Chem Soc* 134:2047–2056.
14. Can TV, Sharma M, Hung I, Gor'kov PL, Brey WW, Cross TA (2012) Magic angle spinning and oriented sample solid-state NMR structural restraints combine for influenza A M2 protein functional insights. *J Am Chem Soc* 134:9022–9025.
15. Miao Y, Qin H, Fu R, Sharma M, Can TV, Hung I, Luca S, Gor'kov PL, Brey WW, Cross TA (2012) M2 proton channel structural validation from full-length protein samples in synthetic bilayers and E. coli membranes. *Angew Chem Int Ed Engl* 51:8383–8386.
16. Park SH, Das BB, Casagrande F, Tian Y, Nothnagel HJ, Chu M, Kiefer H, Maier K, DeAngelis AA, Marassi FM, Opella SJ (2012) Structure of the chemokine receptor CXCR1 in phospholipid bilayers. *Nature* 491:779–783.
17. Holsinger LJ, Shaughnessy MA, Micko A, Pinto LH, Lamb RA (1995) Analysis of the posttranslational modifications of the influenza virus M2 protein. *J Virol* 69:1219–1225.
18. Ma C, Polishchuk AL, Ohigashi Y, Stouffer AL, Schon A, Magavern E, Jing X, Lear JD, Freire E, Lamb RA, DeGrado WF, Pinto LH (2009) Identification of the functional core of the influenza A virus A/M2 proton-selective ion channel. *Proc Natl Acad Sci USA* 106:12283–12288.
19. Sharma M, Yi M, Dong H, Qin H, Peterson E, Busath DD, Zhou HX, Cross TA (2010) Insight into the mechanism of the influenza A proton channel from a structure in a lipid bilayer. *Science* 330:509–512.
20. Jin H, Lesser GP, Zhang J, Lamb RA (1997) Influenza virus hemagglutinin and neuraminidase cytoplasmic tails control particle shape. *EMBO J* 16:1236–1247.
21. Pinto LH, Holsinger LJ, Lamb RA (1992) Influenza virus M2 protein has ion channel activity. *Cell* 69:517–528.
22. Rossman JS, Jing X, Leser GP, Lamb RA (2010) Influenza virus M2 protein mediates ESCRT-independent membrane scission. *Cell* 142:902–913.
23. Rossman JS, Lamb RA (2011) Influenza virus assembly and budding. *Virology* 411:229–236.
24. Pinto LH, Lamb RA (2006) The M2 proton channels of influenza A and B viruses. *J Biol Chem* 281:8997–9000.
25. Wang J, Pielak RM, McClintock MA, Chou JJ (2009) Solution structure and functional analysis of the influenza B proton channel. *Nat Struct Mol Biol* 16:1267–1271.
26. Li H, Papadopoulos V (1997) Peripheral-type benzodiazepine receptor function in cholesterol transport. Identification of a putative cholesterol recognition/interaction amino acid sequence and consensus pattern. *Endocrinology* 139:4991–4997.
27. Cherezov V, Rosenbaum DM, Hanson MA, Rasmussen SG, Thian FS, Kobilka TS, Choi HJ, Kuhn P, Weis WI, Kobilka BK, Stevens RC (2007) High-resolution crystal structure of an engineered human beta2-adrenergic G protein-coupled receptor. *Science* 318:1258–1265.
28. Cross TA, Dong H, Sharma M, Busath DD, Zhou HX (2012) M2 protein from influenza A: from multiple structures to biophysical and functional insights. *Curr Opin Virol* 2:128–133.
29. Sansom MS, Kerr ID (1993) Influenza virus M2 protein: a molecular modelling study of the ion channel. *Protein Eng* 6:65–74.
30. Sansom MS, Kerr ID, Smith GR, Son HS (1997) The influenza A virus M2 channel: a molecular modeling and simulation study. *Virology* 233:163–173.
31. Pinto LH, Dieckmann GR, Gandhi CS, Papworth CG, Braman J, Shaughnessy MA, Lear JD, Lamb RA, DeGrado WF (1997) A functionally defined model for the M2 proton channel of influenza A virus suggests a mechanism for its ion selectivity. *Proc Natl Acad Sci USA* 94:11301–11306.
32. Kukol A, Adams PD, Rice LM, Brunger AT, Arkin TI (1999) Experimentally based orientational refinement of membrane protein models: a structure for the Influenza A M2 H<sup>+</sup> channel. *J Mol Biol* 286:951–962.
33. Wang J, Kim S, Kovacs F, Cross TA (2001) Structure of the transmembrane region of the M2 protein H(+) channel. *Protein Sci* 10:2241–2250.
34. Nishimura K, Kim S, Zhang L, and Cross, T.A (2002) The closed state of a H<sup>+</sup> channel helical bundle: combining precise orientational and distance restraints from solid state NMR. *Biochemistry* 41:13170–13177.
35. Bauer CM, Pinto LH, Cross TA, Lamb RA (1999) The influenza virus M2 ion channel protein: probing the structure of the transmembrane domain in intact cells by using engineered disulfide cross-linking. *Virology* 254:196–209.
36. Hu J, Asbury T, Achuthan S, Li C, Bertram R, Quine JR, Fu R, Cross TA (2007) Backbone structure of the amantadine-blocked trans-membrane domain M2 proton channel from Influenza A virus. *Biophys J* 92:4335–4343.
37. Yi M, Cross TA, Zhou HX (2008) A secondary gate as a mechanism for inhibition of the M2 proton channel by amantadine. *J Phys Chem B* 112:7977–7979.
38. Cady SD, Schmidt-Rohr K, Wang J, Soto CS, DeGrado WF, Hong M (2010) Structure of the amantadine binding site of influenza M2 proton channels in lipid bilayers. *Nature* 463:689–692.
39. Stouffer AL, Acharya R, Salom D, Levine AS, Di Costanzo L, Soto CS, Tereshko V, Nanda V, Stayrook S, DeGrado WF (2008) Structural basis for the function and inhibition of an influenza virus proton channel. *Nature* 451:596–599.
40. Acharya R, Carnevale V, Fiorin G, Levine BG, Polishchuk AL, Balannik V, Samish I, Lamb RA, Pinto LH, DeGrado WF, Klein ML (2010) Structure and mechanism of proton transport through the transmembrane tetrameric M2 protein bundle of the influenza A virus. *Proc Natl Acad Sci USA* 107:15075–15080.
41. Hu J, Fu R, Nishimura K, Zhang L, Zhou HX, Busath DD, Vijayvergiya V, Cross TA (2006) Histidines, heart of the hydrogen ion channel from influenza A virus: toward an understanding of conductance and proton selectivity. *Proc Natl Acad Sci USA* 103:6865–6870.
42. Schnell JR, Chou JJ (2008) Structure and mechanism of the M2 proton channel of influenza A virus. *Nature* 451:591–595.
43. Tian C, Gao PF, Pinto LH, Lamb RA, Cross TA (2003) Initial structural and dynamic characterization of the M2 protein transmembrane and amphipathic helices in lipid bilayers. *Protein Sci* 12:2597–2605.
44. Sharma M, Li C, Busath DD, Zhou HX, Cross TA (2011) Drug sensitivity, drug-resistant mutations, and structures of three conductance domains of viral porins. *Biochim Biophys Acta* 1808:538–546.

45. Pielak RM, Chou JJ (2010) Solution NMR structure of the V27A drug resistant mutant of influenza A M2 channel. *Biochem Biophys Res Commun* 401:58–63.
46. Pielak RM, Oxenoid K, Chou JJ (2011) Structural investigation of rimantadine inhibition of the AM2-BM2 chimera channel of influenza viruses. *Structure* 19:1655–1663.
47. Gullingsrud J, Schulten K (2004) Lipid bilayer pressure profiles and mechanosensitive channel gating. *Biophys J* 86:3496–3509.
48. Cady SD, Hong M (2008) Amantadine-induced conformational and dynamical changes of the influenza M2 transmembrane proton channel. *Proc Natl Acad Sci USA* 105:1483–1488.
49. Cady SD, Mishanina TV, Hong M (2009) Structure of amantadine-bound M2 transmembrane peptide of influenza A in lipid bilayers from magic-angle-spinning solid-state NMR: the role of Ser31 in amantadine binding. *J Mol Biol* 385:1127–1141.
50. Tu Q, Pinto LH, Luo G, Shaughnessy MA, Mullaney D, Kurtz S, Krystal M, Lamb RA (1996) Characterization of inhibition of M2 ion channel activity by BL-1743, an inhibitor of Influenza A virus. *J Virol* 70:4246–4252.
51. Wang C, Takeuchi K, Pinto LH, Lamb RA (1993) Ion channel activity of influenza A virus M2 protein: characterizations of the amantadine block. *J Virol* 67:5585–5594.
52. Cady S, Wang T, Hong M (2011) Membrane-dependent effects of a cytoplasmic helix on the structure and drug binding of the influenza virus M2 protein. *J Am Chem Soc* 133:11572–11579.
53. Chen H, Wu Y, Voth GA (2007) Proton transport behavior through the influenza A M2 channel: insights from molecular simulation. *Biophys J* 93:3470–3479.
54. Khurana E, Devane RH, Dal Peraro M, Klein ML (2011) Computational study of drug binding to the membrane-bound tetrameric M2 peptide bundle from Influenza A virus. *Biochim Biophys Acta* 1808:530–537.
55. Astrahan P, Kass I, Cooper MA, Arkin IT (2004) A novel method of resistance for influenza against a channel-blocking antiviral drug. *Proteins* 55:251–257.
56. Du J, Cross TA, Zhou HX (2012) Recent progress in structure-based anti-influenza drug design. *Drug Discov Today* 17:1111–1120.
57. Wang J, Ma C, Fiorin G, Carnevale V, Wang T, Hu F, Lamb RA, Pinto LH, Hong M, Klein ML, DeGrado WF (2011) Molecular dynamics simulation directed rational design of inhibitors targeting drug-resistant mutants of influenza A virus M2. *J Am Chem Soc* 133:12834–12841.
58. Salom D, Hill BR, Lear JD, DeGrado WF (2000) pH-dependent tetramerization and amantadine binding of the transmembrane helix of M2 from the influenza A virus. *Biochemistry* 39:14160–14170.
59. Wang C, Lamb RA, Pinto LH (1995) Activation of the M2 ion channel of influenza virus: a role for the transmembrane domain histidine residue. *Biophys J* 69:1363–1371.
60. Song X-J, Rienstra, C.M. & McDermott, A.E. (2001) N-H bond stretching in histidine complexes: a solid-state NMR study. *Magn Reson Chem* 39:S30–S36.
61. Hu F, Schmidt-Rohr K, Hong M (2012) NMR detection of pH-dependent histidine-water proton exchange reveals the conduction mechanism of a transmembrane proton channel. *J Am Chem Soc* 134:3703–3713.
62. Duong-Ly KC, Nanda V, DeGrado WF, Howard KP (2005) The conformation of the pore region of the M2 proton channel depends on lipid bilayer environment. *Protein Sci* 14:856–861.
63. Hong M, DeGrado WF (2012) Structural basis for proton conduction and inhibition by the influenza M2 protein. *Protein Sci* 21:1620–1633.
64. Zhang J, Pekosz A, Lamb RA (2000) Influenza virus assembly and lipid raft microdomains: a role for the cytoplasmic tails of the spike glycoproteins. *J Virol* 74:4634–4644.
65. Schroeder C, Heider H, Moncke-Buchner E, Lin TI (2005) The influenza virus ion channel and maturation cofactor M2 is a cholesterol-binding protein. *Eur Biophys J* 34:52–66.
66. Zebedee SL, Lamb RA (1988) Influenza A virus M2 protein: monoclonal antibody restriction of virus growth and detection of M2 in virions. *J Virol* 62:2762–2772.
67. Andreas LB, Eddy MT, Pielak RM, Chou J, Griffin RG (2010) Magic angle spinning NMR investigation of influenza A M2(18–60): support for an allosteric mechanism of inhibition. *J Am Chem Soc* 132:10958–10960.
68. Kass I, Arkin IT (2005) How pH opens a H<sup>+</sup> channel: the gating mechanism of Influenza A M2. *Structure* 13:1789–1798.
69. Wu Y, Voth GA (2005) A computational study of the closed and open states of the influenza A M2 proton channel. *Biophys J* 89:2402–2411.
70. Mould JA, Li H-C, Dudlak CS, Lear JD, Pekosz A, Lamb RA, Pinto LH (2000) Mechanism for proton conduction of the M2 ion channel of Influenza A virus. *J Biol Chem* 275:8592–8599.
71. Lin T, Schroeder C (2001) Definitive assignment of proton selectivity and attoampere unitary current to the M2 ion channel protein of influenza A virus. *J Virol* 75:3647–3656.
72. Pielak RM, Chou JJ (2010) Kinetic analysis of the M2 proton conduction of the influenza virus. *J Am Chem Soc* 132:17695–17697.
73. Peterson E, Ryser T, Funk S, Inouye D, Sharma M, Qin H, Cross TA, Busath DD (2011) Functional reconstitution of influenza A M2(22–62). *Biochim Biophys Acta* 1808:516–521.
74. Leiding T, Wang J, Martinsson J, DeGrado WF, Arskold SP (2010) Proton and cation transport activity of the M2 proton channel from influenza A virus. *Proc Natl Acad Sci USA* 107:15409–15414.
75. Yi M, Cross TA, Zhou HX (2009) Conformational heterogeneity of the M2 proton channel and a structural model for channel activation. *Proc Natl Acad Sci USA* 106:13311–13316.
76. Khurana E, Dal Peraro M, DeVane R, Vemparala S, DeGrado WF, Klein ML (2009) Molecular dynamics calculations suggest a conduction mechanism for the M2 proton channel from influenza A virus. *Proc Natl Acad Sci USA* 106:1069–1074.
77. Zhou HX (2010) Diffusion-influenced transport of ions across a transmembrane channel with an internal binding site. *J Phys Chem Lett* 1:1973–1976.
78. Zhou HX (2011) A theory for the proton transport of the influenza virus M2 protein: extensive test against conductance data. *Biophys J* 100:912–921.
79. Chizhnikov IV, Geraghty FM, Ogden DC, Hayhurst A, Antoniou M, Hay AJ (1996) Selective proton permeability and pH regulation of the influenza virus M2 channel expressed in mouse erythrocyte cells. *J Physiol* 494:329–336.
80. Chizhnikov IV, Ogden DC, Geraghty FM, Hayhurst A, Skinner A, Betakova T, Hay AJ (2003) Differences in conductance of M2 proton channels of two influenza viruses at low and high pH. *J Physiol* 546:427–438.
81. Zhou HX (2011) Mechanistic insight into the H<sub>2</sub>O/D<sub>2</sub>O isotope effect in the proton transport of the influenza virus m2 protein. *J Membr Biol* 244:93–96.